https://dx.doi.org/10.1016/j.ijmecsci.2018.08.028
This is the Pre-Published Version.

Nonlocal scale effect on Rayleigh wave propagation in porous fluid-saturated materials

L.H. Tong[a], S.K. Lai[b,c,*], L.L. Zeng[a], C.J. Xu[a], J. Yang[d]

[a] *Jiangxi Key Laboratory of Infrastructure Safety and Control in Geotechnical Engineering, East China Jiaotong University, Nanchang, Jiangxi, P.R. China*

[b] *Department of Civil and Environmental Engineering, The Hong Kong Polytechnic University, Hung Hom, Kowloon, Hong Kong, P.R. China*

[c] *The Hong Kong Polytechnic University Shenzhen Research Institute, Shenzhen, P.R. China*

[d] *School of Engineering, RMIT University, PO Box 71, Bundoora, VIC 3083 Australia*

Abstract

In this paper, a Rayleigh wave model in fluid saturated porous materials based on a nonlocal Biot theory is proposed. The general characteristic equations expressed in terms of the Rayleigh wavenumbers are obtained. A specific fluid saturated porous material is used for numerical analysis. The present study shows that the nonlocal parameter does not have significant influence on the characteristics of Rayleigh waves within a low frequency range when comparing with the prediction of using the classical Biot theory. However, the influence of the nonlocal scale effect on the Rayleigh wave velocity and the displacement field becomes stronger as the response frequency increases. When the frequency exceeds a critical value, the Rayleigh wave velocity exhibits a negative dispersion. The displacement fields induced by the Rayleigh wave propagating in porous materials are also presented. An interesting phenomenon of the

*Corresponding author. *E-mail address:* sk.lai@polyu.edu.hk (S.K. Lai)

© 2018. This manuscript version is made available under the CC-BY-NC-ND 4.0 license http://creativecommons.org/licenses/by-nc-nd/4.0/

displacement fields is observed that the major axis of the displacement field ellipse will have a contra-rotation with respect to the vertical direction with increasing depth. This is different from the classical prediction in homogeneous materials. The presence of the nonlocal scale effect can also change the geometry property of displacement fields. In addition, the amplitude of the vertical displacement is attenuated along the depth, while the increment of the nonlocal parameters can strengthen the attenuation.

Keywords: Nonlocal Biot theory, Rayleigh waves, Fluid saturated, Porous materials

1. Introduction

Porous materials, such as water saturated soils or sedimentary rocks, are frequently studied in geophysical and earthquake engineering [1, 2]. Moreover, air filled porous metals that have excellent potential applications in aero-engineering [3, 4] can also be found in a variety of engineering fields. Aimed at implementing the problems on deformation and dynamical characteristics of porous materials, Biot proposed a series of pioneering works [5-9], laying a solid theoretical foundation to investigate porous materials. A considerable number of works on porous materials have been reported since the experimental verification of the Biot theory by Plona in 1980 [10]. Afterwards, there were many intensive studies on the bulk wave characteristics [11-16] in porous materials, and much research efforts have also focused on Rayleigh surface waves in accordance with the Biot theory [17-22].

Rayleigh surface waves are formed by the interaction of both compression and shear waves [23]. As a result, the surface waves carry abundant information of the mechanical and dynamical properties of media where it propagates. Among the potential applications, it is capable of estimating the shear wave velocity and the quality factor by the inversion of surface waves [24, 25]. It is also useful for the design of detecting landmines [26, 27]. Hence, understanding the characteristics of Rayleigh surface waves is highly essential in nature.

The dispersion of Rayleigh waves in porous media has been studied intensively in the past few decades. By simplifying the Biot theory and neglecting the inertia coupling between fluids and solids, Jones [28] first investigated the propagation of Rayleigh

surface waves in a fluid saturated solid and indicated that there exists at least one type of Rayleigh waves for the case where the constant relates to Darcy's permeability b = 0. However, Tajuddin [29] pointed out that the solutions obtained by Jones [28] were incorrect by re-addressing this problem. He further extended the wave velocity equation for an impervious surface, the relationship between the surface wave velocity and the Poisson's ratio was also given. Allard et al. [30] experimentally investigated the propagation of Rayleigh-type surface waves at an air-air saturated porous layer interface, and the corresponding application on the metrology of porous media was suggested. Besides, the asymptotic behavior of surface waves at a vacuum/porous medium interface under the low frequency range was implemented by Edelman [31]. Based on this study, the existence of two types of surface waves was proved, i.e., the common Rayleigh wave with almost no attenuation and the special Stoneley wave with a strong attenuation. To investigate the dispersion relation of surface waves over a full frequency range, Albers and Wilmanski [32] developed a simplified linear two-component poro-elastic medium model. Both the Rayleigh and Stoneley waves were predicted by their models for the impervious boundary of saturated poro-elastic media [32], and a similar conclusion was drawn by Edelman [31]. Under the framework of a variational formulation, Placidi et al. [33] proposed a pre-stressed solid-fluid mixture theory that can also be used to investigate the propagation of Rayleigh-type surface waves in pre-stressed fluid saturated porous media.

To consider the effect of double-porosity media, Dai et al. [18] studied the dispersion and attenuation properties of Rayleigh waves under a permeable boundary

by neglecting the coupling mass coefficient and the coupling permeability term. Recently, the equivalent-viscoelastic representation of a fluid-saturated model was proposed by Zhang et al. [20]. They obtained both the waveform and dispersion solutions within the low frequency range in a homogeneous half-space. In addition, the propagation characteristics of Rayleigh waves in non-homogeneous and orthotropic fluid-saturated porous media were also investigated [22, 34]. In the literature, the propagation of surface waves in unsaturated poro-elastic media can also be found in some scattering works [17, 19, 35].

A well-known wave property of saturated porous materials is the appearance of second compression waves [36]. This makes the characteristics of Rayleigh waves propagating in porous media become much more complicated. The use of numerical approaches frequently encounters difficulties such as convergence problems and computational consumptions [20]. Therefore, the development of an efficient analytical model is highly desired. From the previous literature, most of the investigations on Rayleigh waves in porous media were presented in accordance with the poro-elastic Biot theory due to its inherent simplicity in real engineering practice. However, the classical Biot theory was built on the simplified assumptions that may be not in conformity with practical circumstances, thereby causing deviations from experimental observations [16]. To relax this constraint, Tong et al. [16] proposed a nonlocal Biot model to improve the classical one by including the effects of pore size and porosity dynamics into the Biot theory. In the context of nonlocal-based models, the linear-elastic constitutive relation is replaced by a nonlocal elastic constitutive relation [37-

43]. It is found that the dispersion of bulk waves predicted by the nonlocal Biot model agrees well with the experimental observations.

In the present article, we extended the previous work [16] to characterize the effect of Rayleigh waves in accordance with the nonlocal Biot theory. The influence of pore size and porosity dynamics on the Rayleigh wave velocity is analyzed, and the quality factor of a fluid saturated porous material is also studied. An illustrative numerical example is given to verify the validity of the nonlocal Biot model. The displacement fields of Rayleigh waves at some specific frequencies are also presented. It is found that the effects of pore size and porosity dynamics contribute a significant impact on the characteristics of Rayleigh waves propagating in fluid saturated porous materials.

2. Formulation of nonlocal Biot model

Consider a fluid saturated porous material with solid grains surrounded by fluid filling in the inter-connected pores with a porosity n_0, the displacement fields of the solid and fluid components are denoted by $\mathbf{u}$ and $\mathbf{U}$ to describe the corresponding motions, respectively. For brevity and convenience, a vector $\mathbf{w} = n_0\left(\mathbf{U}-\mathbf{u}\right)$ is introduced to characterize the relative displacement between solids and fluids. By neglecting the body force, the fundamental governing equations for a linear, homogeneous, isotropic and nonlocal poro-elastic material are given by [16],

$$\begin{aligned}
&\left(1-\tau^2\nabla^2\right)\left(\rho\ddot{\mathbf{u}}+\rho_f\ddot{\mathbf{w}}\right)=\mu\nabla^2\mathbf{u}+\left(\lambda+\alpha^2M+\mu\right)\operatorname{grad}e-\alpha M\operatorname{grad}\zeta\\
&\rho_f\ddot{\mathbf{u}}+m\ddot{\mathbf{w}}+\frac{\eta}{\kappa}F\left(\varsigma\right)\dot{\mathbf{w}}=\operatorname{grad}\left(\alpha Me-M\zeta\right)
\end{aligned}\tag{1}$$

where τ is the nonlocal parameter that was elaborated in the previous work [16]; $e=\varepsilon_{ii}$ with $\boldsymbol{\varepsilon}=\nabla\mathbf{u}$; $\zeta=-\operatorname{div}\mathbf{w}$ is the variation of fluid content per a unit reference

volume with div the divergence operator; $\rho=(1-n_0)\rho_s+n_0\rho_f$ with ρ_s the mass density of the solid and ρ_f the mass density of the pore fluid; κ is the permeability; $m=\tilde{\alpha}\rho_f/n_0$ with $\tilde{\alpha}$ the dynamic tortuosity; $\eta=\eta_0 F(\varsigma)$ is the frequency-dependent fluid viscosity with $F(\varsigma)$ the viscosity correction factor as discussed in Ref. [16].

Indeed, the nonlocal stress in Eq. (1) is referred to the total stress of a bulk material σ [16], i.e., the total stress satisfies the condition $(1-\tau^2\nabla^2)\sigma=\sigma^L$ where σ^L is the local total stress. It is well known that the total stress is contributed by two parts σ^s and σ^f [8]. The component σ^s represents a force applied to the solid part of the faces, while σ^f denotes a force applied to the fluid part of these faces that can also be expressed by $\sigma^f=-n_0 p_f$ with p_f the pore water pressure. When the nonlocal effect is included into the model, the fluid saturated material can be viewed as a statistical average single system. One may argue that the nonlocal effect must be applied on both solid and fluid components separately. However, it should be emphasized that the nonlocal effect considered herein is used to reflect the influence of pore size on the dynamic response of the total solid-fluid system. If the nonlocal effect is only considered in a single phase, i.e. solid or fluid phase, the entire coupled system is manually separated. Hence, the emphasis is transferred to the dynamic response of the single solid or fluid component but not the total system. Then, the effect of pore size on the total system is hard to be captured. To investigate the influence of pore size on the dynamic response of the total system, the governing equation (1) must be used and combined with the boundary conditions for incompressible constituents or compressible constituents [44] for further analysis.

In addition, it is worth noting that the viscosity correction factor cannot be

neglected for the frequency that exceeds a critical value due to the invalidity of the Poiseuille flow assumption [7]. For a water saturated porous material with a pore radius of 100 μm , the critical frequency is around at 127 Hz that commonly exceeds in practical engineering problems. The parameter M is dependent on the bulk modulus that can be expressed as [16]

$$\begin{aligned} &M = Q/\left[n_0 \left(\alpha - n_0 \right) \right], \\ &\alpha = 1 - K_b / K_s , \\ &Q = \frac{n_0 K_s \left(K_s - n_0 K_s - K_b \right)}{K_s + \gamma K_s^{\,2} - K_b}, \\ &\gamma = n_0 \left(1/K_f - 1/K_s \right) \end{aligned} \tag{2}$$

where K_b is the frame bulk modulus; K_f and K_s are the fluid bulk modulus and the solid bulk modulus, respectively.

A standard simplification process on Eq. (1) is to re-write the displacement fields by introducing the following scalar and vector potentials [29]

$$\mathbf{u} = \nabla \varphi_1 + \nabla \times \boldsymbol{\psi}_1, \quad \mathbf{w} = \nabla \varphi_2 + \nabla \times \boldsymbol{\psi}_2 \tag{3}$$

where $\varphi_i \left(i = 1, 2 \right)$ and $\boldsymbol{\psi}_i \left(i = 1, 2 \right)$ are the scaler and vector potentials, respectively. The subscripts 1 and 2 denote the quantities related to solids and fluids, respectively. For a dynamical response in a half-space, only two directions should be considered, they are assumed as the *x*-direction and *z*-direction. Then, Eq. (3) is expressed as,

$$\begin{aligned} &u_x = \frac{\partial \varphi_1}{\partial x} - \frac{\partial \psi_{12}}{\partial z}, u_z = \frac{\partial \varphi_1}{\partial z} + \frac{\partial \psi_{12}}{\partial x} \\ &w_x = \frac{\partial \varphi_2}{\partial x} - \frac{\partial \psi_{22}}{\partial z}, u_z = \frac{\partial \varphi_2}{\partial z} + \frac{\partial \psi_{22}}{\partial x} \end{aligned} \tag{4}$$

where ψ_{12} and ψ_{22} are the second components of the vectors $\boldsymbol{\psi}_1$ and $\boldsymbol{\psi}_2$, respectively. For brevity, ψ_{12} and ψ_{22} are replaced by the notations ψ_1 and ψ_2 in the following content. Substitute Eq. (4) into Eq. (1) and manipulate a simple

mathematical procedure to eliminate $\psi_i\left(i=1,2\right)$, the following governing equations can be obtained

$$\begin{aligned}&\left(\lambda+2\mu+\alpha^2M\right)\nabla^2\varphi_1+\alpha M\nabla^2\varphi_2+\rho\tau^2\nabla^2\ddot{\varphi}_1+\rho_f\tau^2\nabla^2\ddot{\varphi}_2-\rho\ddot{\varphi}_1-\rho_f\ddot{\varphi}_2=0\\&\alpha M\nabla^2\varphi_1+M\nabla^2\varphi_2-\rho_f\ddot{\varphi}_1-m\ddot{\varphi}_2-\frac{\eta F\left(\varsigma\right)}{\kappa}\dot{\varphi}_2=0\end{aligned}\tag{5}$$

Consider a harmonic plane wave travelling in the *x*-direction, the solutions to Eq. (5) can be assumed as:

$$\begin{aligned}&\varphi_i=F_i\left(z\right)e^{j(\omega t-kx)}\quad\left(i=1,2\right)\\&\psi_i=G_i\left(z\right)e^{j(\omega t-kx)}\quad\left(i=1,2\right)\end{aligned}\tag{6}$$

where *k* is the wavenumber and ω is the angular frequency of the wave. Substituting $\varphi_i\left(i=1,2\right)$ of Eq.(6) into Eq.(5) yields

$$\begin{aligned}&\frac{\lambda+2\mu+\alpha^2M-\rho\tau^2\omega^2}{\alpha M-\rho_f\tau^2\omega^2}\nabla^2\varphi_1+\nabla^2\varphi_2+\frac{\omega^2}{\alpha M-\rho_f\tau^2\omega^2}\left(\rho\varphi_1+\rho_f\varphi_2\right)=0\\&\alpha\nabla^2\varphi_1+\nabla^2\varphi_2+\frac{\rho_f\omega^2}{M}\varphi_1+\frac{m\omega^2-\dfrac{j\omega\eta F\left(\varsigma\right)}{\kappa}}{M}\varphi_2=0\end{aligned}\tag{7}$$

Eliminate φ_2 from Eq. (7) to obtain a fourth-order equation in terms of φ_1 as

$$\nabla^4\varphi_1+\beta_5\omega^2\nabla^2\varphi_1+\beta_6\omega^4\varphi_1=0\tag{8}$$

where the notations $\beta_i\left(i=1-6\right)$ are defined as

$$\beta_1=\frac{\lambda+2\mu+\alpha^2M-\rho\tau^2\omega^2}{\alpha M-\rho_f\tau^2\omega^2}-\alpha,\quad\beta_4=\frac{m-j\eta F\left(\varsigma\right)/\left(\kappa\omega\right)}{M}$$

$$\beta_2=\frac{\rho}{\alpha M-\rho_f\tau^2\omega^2}-\frac{\rho_f}{M},\qquad\beta_5=\frac{\beta_2}{\beta_1}+\beta_4-\frac{\alpha\beta_3}{\beta_1}$$

$$\beta_3=\frac{\rho_f}{\alpha M-\rho_f\tau^2\omega^2}-\beta_4,\qquad\beta_6=\frac{\beta_2\beta_4}{\beta_1}-\frac{\rho_f\beta_3}{\beta_1M}$$

Further expanding Eq. (8), we obtain a fourth-order equation in terms of $F_1\left(z\right)$ as

$$\left(\frac{d^2}{dz^2}+k^2s_1^{\,2}\right)\left(\frac{d^2}{dz^2}+k^2s_2^{\,2}\right)F_1\left(z\right)=0\tag{9}$$

where $s_i^{\,2}=\left(k_i^{\,2}/k^2\right)-1$, *i*=1,2. k_1 and k_2 that satisfy the equations $k_1^2+k_2^2=\beta_5\omega^2$

and $k_1^2 k_2^2 = \beta_6 \omega^4$ are the wavenumbers of the fast and slow bulk waves. The solution of Eq. (9) can be obtained under the condition of no upward traveling wave as

$$F_1(z) = A_1 e^{jks_1 z} + A_2 e^{jks_2 z} \tag{10}$$

where A_1 and A_2 are constants. Using the second equation in Eq.(7), we determine the expression of $F_2(z)$ as

$$F_2(z) = A_1 B_1 e^{jks_1 z} + A_2 B_2 e^{jks_2 z} \tag{11}$$

where $B_i = \left(1 + s_i^2\right) \dfrac{\beta_1 k^2}{\beta_3 \omega^2} - \dfrac{\beta_2}{\beta_3}$, i=1,2.

Substitute Eq. (4) into Eq. (1) and eliminate $\varphi_i \left(i = 1,2\right)$, the following governing equation in terms of $\psi_i \left(i = 1,2\right)$ can be obtained

$$\begin{aligned} &\left(\mu - \rho\tau^2\omega^2\right)\nabla^2\psi_1 - \rho_f \tau^2 \omega^2 \nabla^2 \psi_2 + \rho\omega^2\psi_1 + \rho_f \omega^2 \psi_2 = 0 \\ &\psi_2 = \frac{\rho_f}{\dfrac{j\eta F(\varsigma)}{\kappa\omega} - m}\psi_1 \end{aligned} \tag{12}$$

By inserting the second equation of Eq. (12) into the first one gives

$$H_1 \nabla^2 \psi_1 + H_2 \omega^2 \psi_1 = 0 \tag{13}$$

where $H_1 = \mu - \rho\tau^2\omega^2 - {\rho_f}^2\tau^2\omega^2 / \left[j\eta F(\varsigma)/(\kappa\omega) - m \right]$ and $H_2 = \rho + {\rho_f}^2 / \left[j\eta/(\kappa\omega) - m \right]$. Obviously, only one shear wave is predicted from Eq. (13). We further expand Eq. (13) to reach an equation in the form of $G_1(z)$ as

$$\frac{d^2 G_z(z)}{dz^2} + \left(\frac{H_2}{H_1}\omega^2 - k^2 \right) G_1(z) = 0 \tag{14}$$

where $s_3^2 = k_s^2 / k^2 - 1$ and $k_s^2 = H_2\omega^2 / H_1$ is the wavenumber of shear waves. Assume that there is no upward travel wave to give the solution to $G_1(z)$ as follows

$$G_1(z) = A_3 e^{jks_3 z} \tag{15}$$

where A_3 is a constant. Then, $G_2(z)$ can be easily determined from Eq.(12)

$$G_2(z) = A_3 B_3 e^{jks_3 z} \tag{16}$$

where $B_3 = \rho_f / \left[j\eta F(\varsigma)/(\kappa\omega) - m \right]$.

3. Rayleigh waves in fluid saturated porous materials

The displacement potentials $\varphi_i (i = 1,2)$ and $\psi_i (i = 1,2)$ are available to explicitly determine the solid and fluid displacement fields using Eq. (4). The constitutive equations of the nonlocal Biot theory is governed by the following relationship [16]

$$\left(1 - \tau^2 \nabla^2\right) \sigma_{ij} = \sigma_{ij}^{\ L} \tag{17}$$

where σ_{ij} is the nonlocal stress and $\sigma_{ij}^{\ L}$ is the local stress or classical stress. Theoretically, the nonlocal stress can be solved according to Eq. (17), as the local stress $\sigma_{ij}^{\ L}$ is known by using the classical constitutive equations proposed by [8]

$$\begin{aligned} \sigma_{ij}^{\ L} &= 2\mu\varepsilon_{ij} + \lambda\delta_{ij} e - \alpha\delta_{ij} p_f \\ p_f &= -\alpha M e + M\zeta \end{aligned} \tag{18}$$

However, it is difficult to obtain an exact analytical expression of the nonlocal stress σ_{ij} from a mathematical point of view. To be a good approximation, a complete and asymptotic representation of the infinite higher-order governing differential equations can be used to replace Eq. (17) as follows [40]

$$\sigma_{ij} = \sigma_{ij}^{\ L} + \sum_{n=1}^{\infty} \tau^{2n} \nabla^{2n} \sigma_{ij}^{\ L} \tag{19}$$

Suppose that the stress wave is a plane wave, thus the local stress can be presented as $\sigma_{11}^{L} = A_0 e^{j(\omega t - kx)}$. On the right-hand side of Eq. (19), the ratio of the i^{th} term $(i = 2,3,\ldots)$ to the first term is $(\tau k)^{2(i-1)}$. The value of the nonlocal parameter τ is typically in the order of 10^{-3} m. The wave number k, by using the soil parameters

presented in the next section, can be calculated as 421 rad/m for the slow wave and 38 rad/m for the fast wave at the response frequency 10 kHz. Therefore, the ratio $(\tau k)^{2(i-1)}$ is significantly small for $i \geq 3$ (i.e., $n \geq 2$ in Eq. (19)), and the higher-order terms can be neglected.

From Eqs. (6), (18) and (19), the higher-order terms in Eq. (19) are omitted and only the first two terms are taken into consideration. The nonlocal stress terms σ_{xz}, σ_{zz} and the pore fluid pressure p_f can be expressed in terms of the displacements as follows:

$$\begin{aligned}
\sigma_{xz} &= \left[\left(1-\tau^2 k_s^{\,2}\right) N_3 A_3 e^{jks_3 z} + \sum_{i=1,2} \left(1-\tau^2 k_i^{\,2}\right) N_i A_i e^{jks_i z} \right] e^{j(\omega t - kx)} \\
\sigma_{zz} &= \left[2\left(1-\tau^2 k_s^{\,2}\right)\left(1-s_3^{\,2}\right) k^2 A_3 e^{jks_3 z} + \sum_{i=1,2} 2\left(1-\tau^2 k_i^{\,2}\right) k^2 s_i A_i e^{jks_i z} \right] \mu e^{j(\omega t - kx)} \\
p_f &= \sum_{i=1,2} \left(\alpha + B_i\right) M k_i^{\,2} A_i e^{jks_i z} e^{j(\omega t - kx)}
\end{aligned} \tag{20}$$

where $N_i = 2\mu k^2 - \left(\lambda + 2\mu + \alpha^2 M + \alpha M B_1\right) k_i^{\,2} \quad (i = 1, 2)$ and $N_3 = -2\mu s_3 k^2$. The boundary conditions at $z = 0$ for a pervious surface are

$$\sigma_{xz} = 0, \ \sigma_{zz} + p_f = 0, \ p_f = 0 \tag{21}$$

while for an impervious surface become

$$\sigma_{xz} = 0, \ \sigma_{zz} + p_f = 0, \ \frac{\partial p_f}{\partial z} = 0 \tag{22}$$

According to Eqs. (20)-(22), two equation sets for the pervious and impervious surfaces are obtained. When we consider the similarity of the Rayleigh wave characteristics under these two conditions, only the Rayleigh wave for the pervious surface is selected for investigation. The existence of the nontrivial solutions for $A_i \left(i = 1, 2, 3\right)$ requires the determinant of the coefficients to be vanished, that is

$$\left|a_{ij}\right| = 0 \ \ (i, j = 1,2,3) \tag{23}$$

where

$$\begin{aligned}
&a_{11} = 2\left(1-\tau^2 k_1^{\,2}\right)s_1, \quad a_{12} = 2\left(1-\tau^2 k_2^{\,2}\right)s_2, \quad a_{13} = \left(1-s_3^{\,2}\right)\left(1-\tau^2 k_s^{\,2}\right)\\
&a_{21} = \left(1-\tau^2 k_1^{\,2}\right)N_1, \quad a_{22} = \left(1-\tau^2 k_2^{\,2}\right)N_2, \quad a_{23} = \left(1-\tau^2 k_s^{\,2}\right)N_3\\
&a_{31} = \left(\alpha + B_1\right)Mk_1^{\,2}, \quad a_{32} = \left(\alpha + B_2\right)Mk_2^{\,2}, \quad a_{33} = 0
\end{aligned}$$

Equation (23) is expressed in terms of the wavenumber k. Once the value of k is found, the Rayleigh wave velocity can be easily determined by $v_R = \omega/\mathrm{Re}(k)$, in which $\mathrm{Re}(k)$ means the real part of k.

Consider that the equation $\left[a_{ij}\right]\left[A_j\right] = 0$ has nontrivial solutions, A_1 and A_2 can be expressed in terms of A_3 as

$$\begin{aligned}
A_1 &= \frac{a_{13}a_{32}}{a_{12}a_{31} - a_{11}a_{32}}A_3 = R_{13}A_3\\
A_2 &= -\frac{a_{13}a_{31}}{a_{12}a_{31} - a_{11}a_{32}}A_3 = R_{23}A_3
\end{aligned} \tag{24}$$

Then, the displacement fields of the solid components can be expressed as

$$\begin{aligned}
u_z &= jk\left(s_1R_{13}e^{jks_1z} + s_2R_{23}e^{jks_2z} - e^{jks_3z}\right)A_3e^{j(\omega t - kx)}\\
u_x &= -jk\left(R_{13}e^{jks_1z} + R_{23}e^{jks_2z} - s_3e^{jks_3z}\right)A_3e^{j(\omega t - kx)}
\end{aligned} \tag{25}$$

The displacement fields of the fluid components can also be worked out through a similar process. In Eq. (25), the amplitudes of the displacement fields are contributed by three parts, the first two parts are originated from the fast wave and the slow wave, while the last part is originated from the shear wave. Numerical analysis indicates that most of the energy from the Rayleigh wave comes from the shear wave, which is the major reason to use the Rayleigh wave for the estimation of the shear-wave velocity [25].

4. Results and Discussion

To fix the idea on the characteristics of Rayleigh waves propagating in a fluid saturated porous material, a specific numerical example is given to show the influence of the nonlocal effect on the characteristics of Rayleigh waves. An ocean sediment with the following properties is selected [16]: $\rho_s = 2650\ \mathrm{kg\,m^{-3}}$, $\rho_f = 1000\ \mathrm{kg\,m^{-3}}$, $K_f = 2.25\mathrm{GPa}$, $K_s = 36\mathrm{GPa}$, $K_b = 43.6\,\mathrm{MPa}$, $\mu = 26.1\mathrm{MPa}$, $\eta_0 = 0.47$, $\kappa = 1\times10^{-10}\,\mathrm{m^2}$, $\eta = 0.001\ \mathrm{Pa\cdot s}$, $\xi = 1$ and $a = 23\mu\mathrm{m}$. It is noted that the tortuosity $\tilde{\alpha}$ in the work [16] was approximately selected as 1 for convenience. However, the value of $\tilde{\alpha}$ is typically larger than 1 according to the analysis of Berryman [45]. A more detailed discussion on the dynamic tortuosity can be found in the work of Johnson et al. [46]. In this work, we use the approximation equation $\tilde{\alpha}=1-r\left(1-1/n_0\right)$ proposed by Berryman [45] to calculate the tortuosity as 1.56. Here we have taken $r = 0.5$ to obtain the value of $\tilde{\alpha}$ as indicated by Berryman [45] that *r* should satisfy the condition $0 \le r \le 1$. Based on the present nonlocal theory, there is another important parameter τ that is used to characterize the effects of pore size and porosity dynamics. The connection of this parameter to the parameter ℓ proposed by Lopatnikov and Cheng [47], which is also used to study the porosity dynamics, was elaborated in the previous study [16]. To establish the relationship between the fluctuation of porosity, the dissipative stress P_ϕ^{diss} and the dynamic stress P_ϕ^{dyn}, we have [16]

$$\begin{aligned} &P_\phi^{dyn} + P_\phi^{diss} = \rho\ell^2\ddot{n} \\ &\nabla\left(P_\phi^{dyn} + P_\phi^{diss}\right) = -\tau^2\nabla^2\left(\rho\ddot{\mathbf{u}} + \rho_f\ddot{\mathbf{w}}\right) \end{aligned} \tag{26}$$

where *n* is the porosity. Following the mathematical procedure in Ref. [16], the ratio of τ and ℓ can be obtained as

$$\frac{\tau^2}{\ell^2}=\frac{\rho n_0\left(1-n_0\right)\left(\left|\varepsilon_{vf}-\varepsilon_{vs}\right|\right)}{\left(1-n_0\right)\rho_s\varepsilon_{vs}+n_0\rho_f\varepsilon_{vf}} \tag{27}$$

in which ε_{vs} and ε_{vf} are the volume strains of solid and fluid, respectively. Taking advantage of Eq. (27) and the parameter ℓ proposed in Ref. [47], the value of the nonlocal parameter τ can be roughly estimated to be less than 10^{-2} m and typically in the order of 10^{-3} m for many soil materials. However, it is difficult to accurately determine the nonlocal parameter value by using Eq. (27), as the exact volume strains for fluid or solid cannot be measured separately. In fact, the nonlocal parameter τ is highly dependent on the porosity and internal structure of porous materials, which can be determined by measuring the dispersion characteristics of longitudinal waves propagating in a saturated porous material, as elaborated in Ref. [16]. In this work, we do not concentrate on the method to obtain a specific value of the nonlocal parameter τ, while we mainly investigate the variation of τ on the characteristics of Rayleigh surface waves in saturated porous media.

In Fig. 1, the Rayleigh wave velocity as a function of the frequency is plotted for various nonlocal parameters. The shear wave velocity is also shown as a reference in Fig. 1(a). According to the variation of the velocity values at different frequencies, the velocity dispersion is divided into three zones, as shown in Fig. 1. Within Zone I, both the shear wave and Rayleigh wave velocities keep almost constant. When the frequency exceeds the first critical frequency (i.e., about 270 Hz – 280 Hz in this example), the velocity increases gradually as the frequency increases. The classical Biot theory indicates that the velocity keeps stable again when the frequency beyond the second critical frequency (i.e., about 1500 Hz in this example). However, the nonlocal Biot

theory predicts a different trend of the velocity variation. For the nonlocal parameter $\tau = 0.001\mathrm{m}$, the Rayleigh wave velocity starts to deviate from the classical prediction as the dispersion enters into Zone III. In Fig. 1(b), this deviation even starts in Zone II when increasing the nonlocal parameter (see the case of $\tau = 0.005\mathrm{m}$, the deviation starts at f = 270 – 280 Hz). To understand this mechanism, we may imagine a box with several layers from bottom to top. Now we fill each layer by using spherical beads, the bead size in each layer from bottom to top gradually decreases, while the bead size is kept to be the same in a single layer. Suppose that a plane harmonic travelling wave is excited on the top and it propagates downward (regardless of the wave reflection), then the wave will slow down gradually because the scattering becomes more and more obvious.

The velocity dispersion of the Rayleigh wave is similar to that of the shear wave as shown in Fig. 1(a). It is because the wave energy of the Rayleigh wave is mainly contributed by the shear wave. To clearly show this effect, the energy percentages contributed by the fast, slow and shear waves in the displacement u_z for different nonlocal parameters are presented in Fig. 2. Obviously, the energy contribution originated from the shear wave is dominant among others. Within the low frequency range, the slow wave has little contribution to the Rayleigh wave. In fact, the energy of the Rayleigh wave contributed by the fast wave is several orders higher than that of the slow wave within the low frequency range. Therefore, the slow wave can be neglected for convenience without causing significant errors in studying practical engineering problems within the low frequency range. As the frequency increases, more and more

energy is contributed by the slow wave, thus it cannot be neglected for the high frequency range. In Fig. 2, it is also found that the distribution of energy contribution from different types of waves is almost independent with the nonlocal effect. The difference for the cases of $\tau = 0\,\mathrm{m}$ and $\tau = 0.005\,\mathrm{m}$ is less than 1% for the frequency range between 1 Hz and 1000 Hz.

To investigate the attenuation property of Rayleigh waves, the following quality factor is introduced.

$$Q^{-1} = 2\left|\frac{\mathrm{Im}(k)}{\mathrm{Re}(k)}\right| \tag{28}$$

and the corresponding loss angle is defined as

$$\theta = \arctan Q^{-1} \tag{29}$$

The loss angle as a function of frequency for various nonlocal parameters is shown in Fig. 3. The nonlocal parameter does not have significant influence on the loss angle within the low frequency range as compared with prediction of using the classical Biot model. Increasing the frequency, a significant discrepancy can be observed. There exists a critical frequency for different nonlocal parameters. Beyond the critical frequency, the loss angle will increase. For $\tau = 0.001\,\mathrm{m}$, the critical frequency is at 10 kHz (is not fully shown in Fig. 3). While for $\tau = 0.005\,\mathrm{m}$, the critical frequency decreases to 2 kHz. The drastic change of the loss angle manifests the high attenuation of Rayleigh waves. In other words, the Rayleigh wave hardly propagates outwards when the frequency exceeds the critical value. This is consistent with the characteristics of shear waves predicted by the previous work [16], i.e., the higher attenuation of shear waves results in the higher attenuation of Rayleigh waves.

Displacement fields induced by the Rayleigh wave predicted at various nonlocal parameters and frequencies are depicted in Fig. 4. The displacement fields in the *x*- and *z*-directions can be calculated by Eq. (25). It is obvious that the displacement fields in porous materials are different from that induced by the Rayleigh wave traveling in homogeneous single-phase materials, even though it is still the same as an elliptical shape. For the displacements in homogeneous materials, the major axis of the ellipse is always along the vertical direction, while the minor axis is always along the horizontal direction at any depth. Nevertheless, the major axis of the displacement ellipse in porous materials will have a contra-rotation with respect to the vertical direction when increasing depth. Within the low frequency and the small nonlocal parameter, the eccentricity of the displacement ellipse decreases with increasing depth, as shown in Fig. 4. It manifests that the phase difference between u_z and u_x is a function of depth. For $\tau = 0.005m$, the displacement ellipse at a frequency of 3000 Hz can only rotate in a very small angle as the depth varies from 0 to $-0.6\lambda_R$. It implies that the depth has a little impact on the eccentricity of the ellipse. Based on the results in Fig. 4, another conclusion can be drawn that the amplitudes of the displacements u_z and u_x are attenuated along the depth.

In Fig. 5, the attenuation of the displacement amplitude u_z for different nonlocal parameters is presented. At the low frequency (f=10 Hz), there is almost no difference between the results of $\tau = 0\,\mathrm{m}$ and $\tau = 0.005\,\mathrm{m}$. While for the high frequency (f = 3000 Hz), a significant discrepancy can be observed for $\tau = 0\,\mathrm{m}$ and $\tau = 0.005\,\mathrm{m}$. This is also revealed in Fig. 4(c) and (d). In Fig. 5(b), the slope of the line for $\tau = 0$ is

sharper than that for $\tau = 0.005m$, which indicates a higher attenuation coefficient for $\tau = 0.005\mathrm{m}$. It implies that the classical Biot theory may underestimate the influence of the depth on Rayleigh waves.

5. Conclusions

Based on the nonlocal Biot theory, a Rayleigh wave model in fluid saturated porous materials is proposed. The general characteristic equations in terms of the Rayleigh wavenumbers are obtained under a permeable surface condition. A specific fluid saturated porous material is selected for numerical analysis. It is found that the nonlocal parameter has a neglected impact on the wave dispersion, as compared with the prediction of using the classical Biot theory within the low frequency range. However, there is a dominant effect on the wave dispersion in the high frequency range. When the frequency exceeds a critical value, the Rayleigh wave velocity decreases with increasing frequency. This effect cannot be predicted by the classical Biot theory. Besides, the energy contribution by the fast, slow and shear waves is also studied. We found that the nonlocal parameter does not have significant influence on the energy distribution and most of the Rayleigh wave energy is contributed by the shear wave. Therefore, the Rayleigh wave is mainly dominated by the shear wave.

In this paper, the influence of nonlocal parameters on the loss angle is also examined. It is found that there is a specific critical frequency, beyond which the Rayleigh wave cannot propagate outwards, corresponding to a certain nonlocal parameter. The displacement fields induced by the Rayleigh wave for various frequencies are also investigated. It is found that the displacement field ellipse is

different from that in a homogeneous material. The major axis of the displacement field ellipse is no longer along the vertical direction because of the phase difference between the vertical and horizontal displacements with increasing depth in porous materials. Besides, it can be predicted that the attenuation of the displacement amplitude is strengthened by an increasing nonlocal parameter. The present study mainly focuses on the case of pervious surface conditions. However, it is easy to extend this work for the condition of impervious surfaces, and it is expected that a similar conclusion can be reached.

Finally, we remark here that the nonlocal scale effect discussed in this paper is mainly induced by the effects of pore size and porosity dynamics, it is not related to the second strain gradient. In fact, the second gradient poro-mechanics can well treat some special phenomena, e.g., capillarity in fluid, plasticity and shear band deformations and so on. This is also an important improvement of the Biot theory for wider applications in practical engineering (see Refs. [33, 44, 48, 49]). A combination of the nonlocal Biot theory with the second gradient poro-mechanics to generalize the Biot model will be studied in future.

Acknowledgements

The work described in this paper was supported by Natural Science Foundation of Jiangxi (20171BAB216047), National Natural Science Foundation of China (Grants No. 11702095 and 11602210) and the Matching Grant from the Hong Kong Polytechnic University (4-BCDS). The Innovation and Technology Commission of the HKSAR Government to the Hong Kong Branch of the National Rail Transit Electrification and Automation Engineering Technology Research Center (Project No. BBY1 and sub-project 1-BBYJ) was also acknowledged.

References

[1] P.A. Johnson, X. Jia, Nonlinear dynamics, granular media and dynamic earthquake triggering, Nature, 437 (2005) 871-874.

[2] P.A. Johnson, H. Savage, M. Knuth, J. Gomberg, C. Marone, Effects of acoustic waves on stick-slip in granular media and implications for earthquakes, Nature, 451 (2008) 57-60.

[3] M.F. Ashby, The properties of foams and lattices, Philos T R Soc A, 364 (2006) 15-30.

[4] X.L. Wang, F. Peng, B.J. Chang, Sound absorption of porous metals at high sound pressure levels, J Acoust Soc Am, 126 (2009) El55-El61.

[5] M.A. Biot, General theory of three-dimensional consolidation, J Appl Phys, 12 (1941) 155-164.

[6] M.A. Biot, Theory of Propagation of Elastic Waves in a Fluid-Saturated Porous Solid .1. Low-Frequency Range, J Acoust Soc Am, 28 (1956) 168-178.

[7] M.A. Biot, Theory of Propagation of Elastic Waves in a Fluid-Saturated Porous Solid .2. Higher Frequency Range, J Acoust Soc Am, 28 (1956) 179-191.

[8] M.A. Biot, Mechanics of Deformation and Acoustic Propagation in Porous Media, J Appl Phys, 33 (1962) 1482-1498.

[9] M.A. Biot, Nonlinear and Semilinear Rheology of Porous Solids, J Geophys Res, 78 (1973) 4924-4937.

[10] T.J. Plona, Observation of a 2nd Bulk Compressional Wave in a Porous-Medium at Ultrasonic Frequencies, Appl Phys Lett, 36 (1980) 259-261.

[11] T.W. Geerits, O. Kelder, Acoustic wave propagation through porous media: Theory and experiments, J Acoust Soc Am, 102 (1997) 2495-2510.

[12] Z.W. Cui, J.X. Liu, K.X. Wang, Elastic waves in non-Newtonian (Maxwell) fluid-saturated porous media, Wave Random Media, 13 (2003) 191-203.

[13] Y. Liu, K. Liu, L.T. Gao, T.X. Yu, Characteristic analysis of wave propagation in anisotropic fluid-saturated porous media, J Sound Vib, 282 (2005) 863-880.

[14] S. Papargyri-Beskou, D. Polyzos, D.E. Beskos, Wave propagation in 3-D poroelastic media including gradient effects, Archive of Applied Mechanics, 82 (2012) 1569-1584.

[15] H.B. Tao, G.B. Liu, K.H. Xie, R.Y. Zheng, Y.B. Deng, Characteristics of Wave Propagation in The Saturated Thermoelastic Porous Medium, Transport Porous Med, 103 (2014) 47-68.

[16] L.H. Tong, Y. Yu, W. Hu, Y. Shi, C. Xu, On wave propagation characteristics in fluid saturated porous materials by a nonlocal Biot theory, J Sound Vib, 379 (2016) 106-118.

[17] G. Chao, D.M.J. Smeulders, M.E.H. van Dongen, Dispersive surface waves along partially saturated porous media, J Acoust Soc Am, 119 (2006) 1347-1355.

[18] Z.J. Dai, Z.B. Kuang, S.X. Zha, Rayleigh waves in a double porosity half-space, J Sound Vib, 298 (2006) 319-332.

[19] W.C. Lo, Propagation and attenuation of Rayleigh waves in a semi-infinite unsaturated poroelastic medium, Advances in Water Resources, 31 (2008) 1399-1410.

[20] Y. Zhang, Y.X. Xu, J.H. Xia, S.X. Zhang, P. Ping, On effective characteristic of Rayleigh surface wave propagation in porous fluid-saturated media at low frequencies, Soil Dyn Earthq Eng, 57 (2014) 94-103.

[21] Q. Ma, F. Zhou, Propagation Conditions of Rayleigh Waves in Nonhomogeneous Saturated Porous Media, Soil Mechanics and Foundation Engineering, 53 (2016) 268-273.

[22] F.X. Zhou, Q. Ma, Propagation of Rayleigh waves in fluid-saturated non-homogeneous soils with the graded solid skeleton distribution, Int J Numer Anal Met, 40 (2016) 1513-1530.

[23] V.A. Eremeyev, G. Rosi, S. Naili, Surface/interfacial anti-plane waves in solids with surface energy, Mech Res Commun, 74 (2016) 8-13.

[24] J.H. Xia, R.D. Miller, C.B. Park, Estimation of near-surface shear-wave velocity by inversion of Rayleigh waves, Geophysics, 64 (1999) 691-700.

[25] J.H. Xia, R.D. Miller, Estimation of Near-surface Shear-wave Velocity and Quality Factor by Inversion of High-frequency Rayleigh Waves, Geophys Dev Ser, 15 (2010) 17-36.

[26] P.D. Norville, W.R. Scott, Time-reversal focusing of elastic surface waves, J Acoust Soc Am, 118 (2005) 735-744.

[27] P.D. Norville, W.R. Scott, Time-reversal focusing of elastic surface waves with an asymmetric surface layer, J Acoust Soc Am, 122 (2007) El95-El100.

[28] J.P. Jones, Rayleigh Waves in a Porous, Elastic, Saturated Solid, J Acoust Soc Am, 33 (1961) 959-962.

[29] M. Tajuddin, Rayleigh waves in a poroelastic half‐space, The Journal of the Acoustical Society of America, 75 (1984) 682-684.

[30] J.F. Allard, G. Jansens, G. Vermeir, W. Lauriks, Frame-borne surface waves in air-saturated porous media, J Acoust Soc Am, 111 (2002) 690-696.

[31] I. Edelman, Surface waves at vacuum/porous medium interface: low frequency range, Wave Motion, 39 (2004) 111-127.

[32] B. Albers, K. Wilmanski, Monochromatic surface waves on impermeable boundaries in two-component poroelastic media, Continuum Mech Therm, 17 (2005) 269-285.

[33] L. Placidi, F. Dell'Isola, N. Ianiro, G. Sciarra, Variational formulation of pre-stressed solid-fluid mixture theory, with an application to wave phenomena, Eur J Mech A-Solid, 27 (2008) 582-606.

[34] P.C. Vinh, A. Aoudia, P.T.H. Giang, Rayleigh waves in orthotropic fluid-saturated porous media, Wave Motion, 61 (2016) 73-82.

[35] Y.S. Chen, W.C. Lo, J.M. Leu, A.H.D. Cheng, Effect of Impermeable Boundaries on the Propagation of Rayleigh Waves in an Unsaturated Poroelastic Half-Space, J Mech, 26 (2010) 501-511.

[36] G. Rosi, L. Placidi, F. dell'Isola, "Fast" and "slow" pressure waves electrically induced by nonlinear coupling in Biot-type porous medium saturated by a nematic liquid crystal, Zeitschrift für angewandte Mathematik und Physik, 68 (2017) 51.

[37] L.L. Ke, Y. Xiang, J. Yang, S. Kitipornchai, Nonlinear free vibration of embedded double-walled carbon nanotubes based on nonlocal Timoshenko beam theory,

Comp Mater Sci, 47 (2009) 409-417.

[38] C.W. Lim, Y. Yang, New Predictions of Size-Dependent Nanoscale Based on Nonlocal Elasticity for Wave Propagation in Carbon Nanotubes, Journal of Computational and Theoretical Nanoscience, 7 (2010) 988-995.

[39] Y. Yang, L.X. Zhang, C.W. Lim, Wave propagation in fluid-filled single-walled carbon nanotube on analytically nonlocal Euler-Bernoulli beam model, J Sound Vib, 331 (2012) 1567-1579.

[40] J.W. Yan, L.H. Tong, C. Li, Y. Zhu, Z.W. Wang, Exact solutions of bending deflections for nano-beams and nano-plates based on nonlocal elasticity theory, Compos Struct, 125 (2015) 304-313.

[41] C.W. Lim, M.Z. Islam, G. Zhang, A nonlocal finite element method for torsional statics and dynamics of circular nanostructures, International Journal of Mechanical Sciences, 94-95 (2015) 232-243.

[42] M. Shaat, A. Abdelkefi, New insights on the applicability of Eringen's nonlocal theory, International Journal of Mechanical Sciences, 121 (2017) 67-75.

[43] C.Y. Wang, J. Zhang, Y.Q. Fei, T. Murmu, Circumferential nonlocal effect on vibrating nanotubules, International Journal of Mechanical Sciences, 58 (2012) 86-90.

[44] F. dell'Isola, M. Guarascio, K. Hutter, A variational approach for the deformation of a saturated porous solid. A second-gradient theory extending Terzaghi's effective stress principle, Archive of Applied Mechanics, 70 (2000) 323-337.

[45] J.G. Berryman, Elastic Wave-Propagation in Fluid-Saturated Porous-Media, J

Acoust Soc Am, 69 (1981) 416-424.

[46] D. Johnson, J. Koplik, R. Dashen, Theory of dynamic permeability and tortuosity in fluid-saturated porous media, Journal of Fluid Mechanics, 176 (1987) 379-402.

[47] S.L. Lopatnikov, A.H.D. Cheng, Macroscopic Lagrangian formulation of poroelasticity with porosity dynamics, J Mech Phys Solids, 52 (2004) 2801-2839.

[48] G. Sciarra, F. dell'Isola, O. Coussy, Second gradient poromechanics, Int J Solids Struct, 44 (2007) 6607-6629.

[49] L. Placidi, U. Andreaus, A.D. Corte, T. Lekszycki, Gedanken experiments for the determination of two-dimensional linear second gradient elasticity coefficients, Zeitschrift für angewandte Mathematik und Physik, 66 (2015) 3699-3725.

Captions of Figures:

Fig.1. (a) Comparison of the velocity of the Rayleigh wave (v_R) and the shear wave (v_S); and (b) Variation of the Rayleigh wave velocity for various nonlocal parameters τ.

Fig. 2. Percentage contribution from the wave energy of the fast, slow and shear waves in the displacement u_z (a) $\tau = 0\,\mathrm{m}$ and (b) $\tau = 0.005\,\mathrm{m}$.

Fig. 3. Loss angle versus frequency for various nonlocal parameters.

Fig. 4. Displacement fields of the Rayleigh wave. (Both the displacement components u_x and u_z are normalized to A_3. λ_R is the Rayleigh wavelength. All centers of the ellipses are moved to (0,0)).

Fig. 5. Comparison of the vertical displacement at different frequencies for nonlocal parameters $\tau = 0\,\mathrm{m}$ and $\tau = 0.005\,\mathrm{m}$.

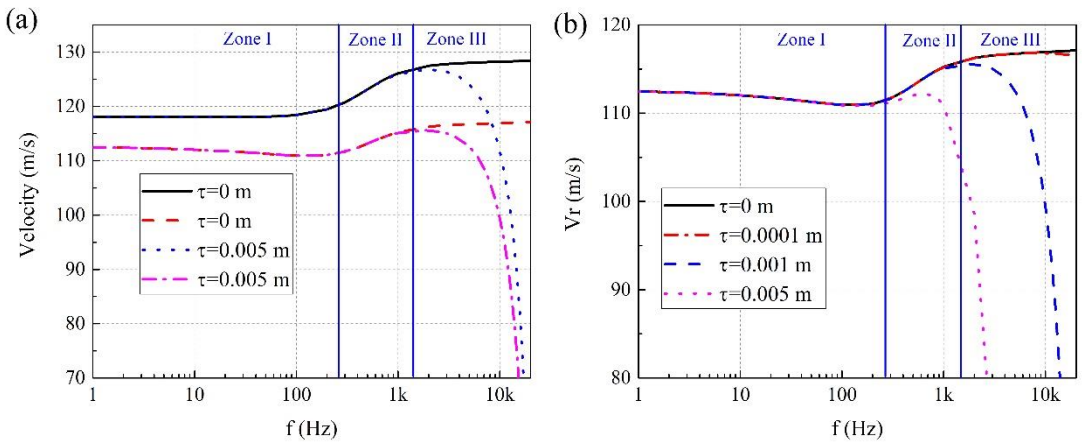

Fig. 1. (a) Comparison of the velocity of the Rayleigh wave (v_R) and the shear wave (v_S); and (b) Variation of the Rayleigh wave velocity for various nonlocal parameters τ.

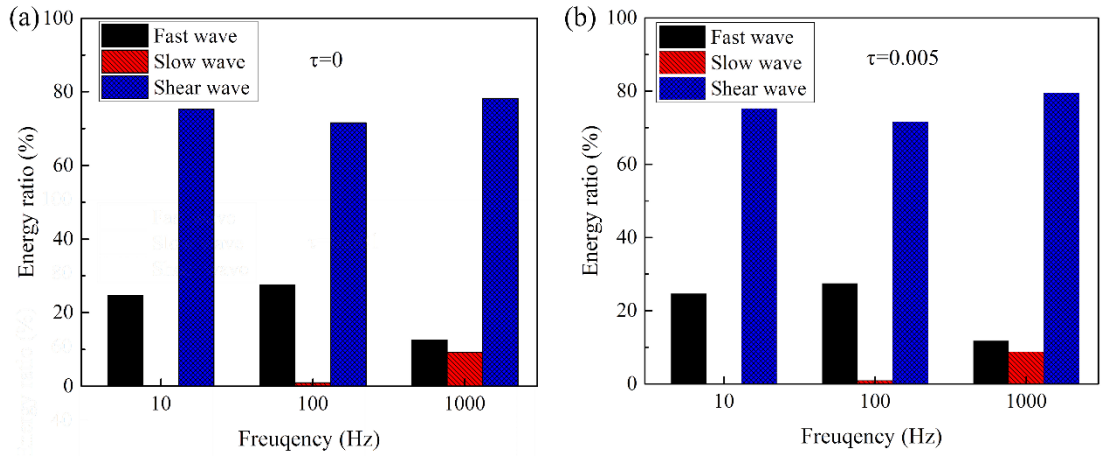

Fig. 2. Percentage contribution from the wave energy of the fast, slow and shear waves in the displacement u_z (a) $\tau = 0\,\mathrm{m}$ and (b) $\tau = 0.005\,\mathrm{m}$.

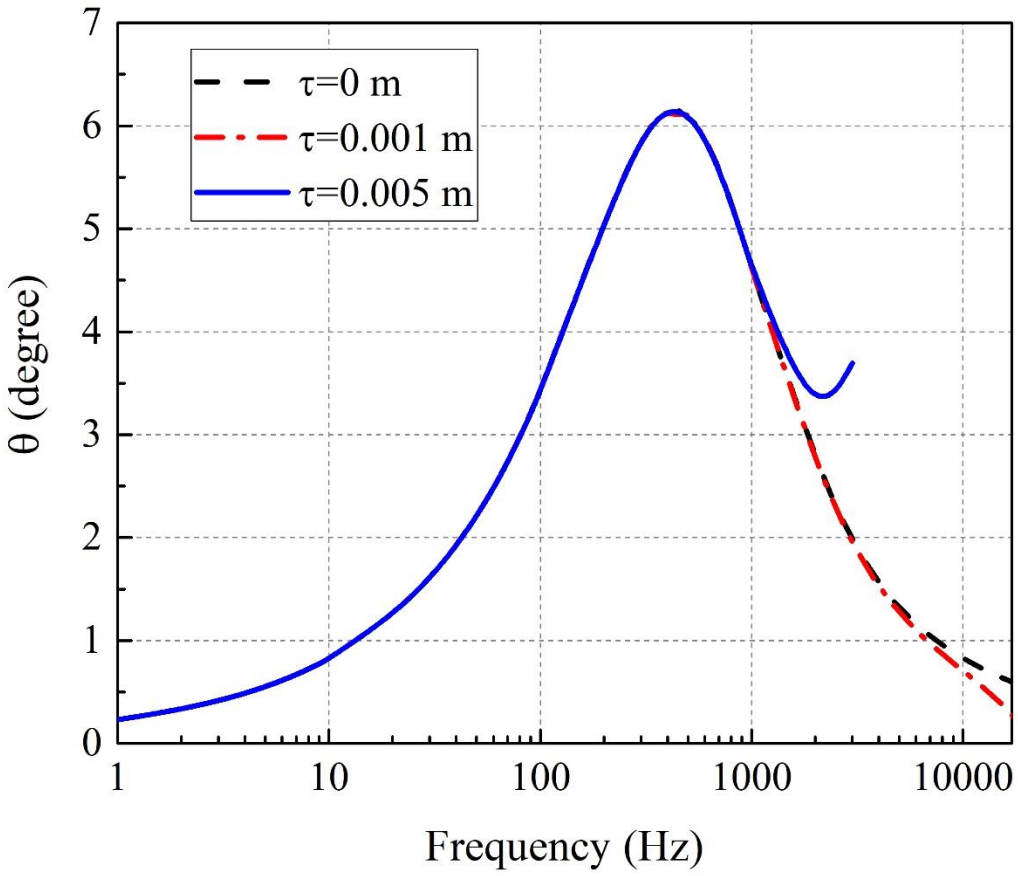

Fig. 3. Loss angle versus frequency for various nonlocal parameters.

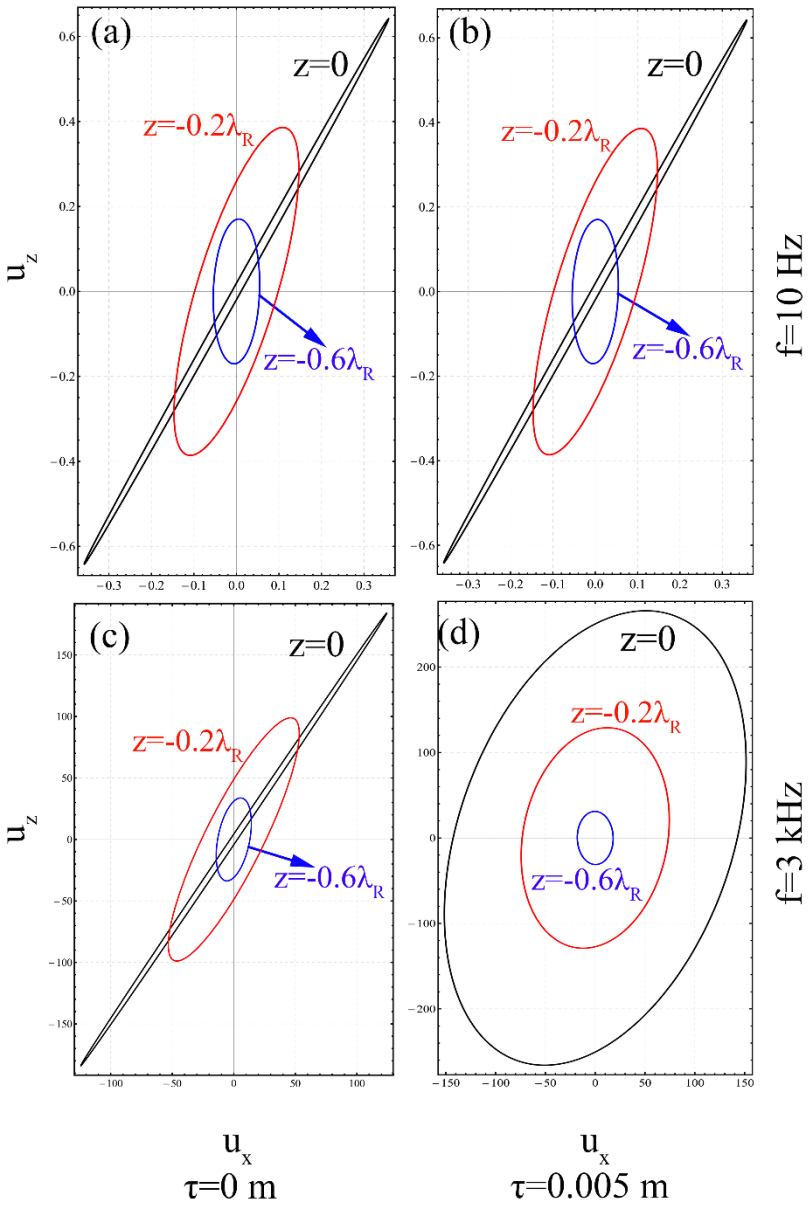

Fig. 4. Displacement fields of the Rayleigh wave. (Both the displacement components u_x and u_z are normalized to A_3. λ_R is the Rayleigh wavelength. All centers of the ellipses are moved to (0,0)).

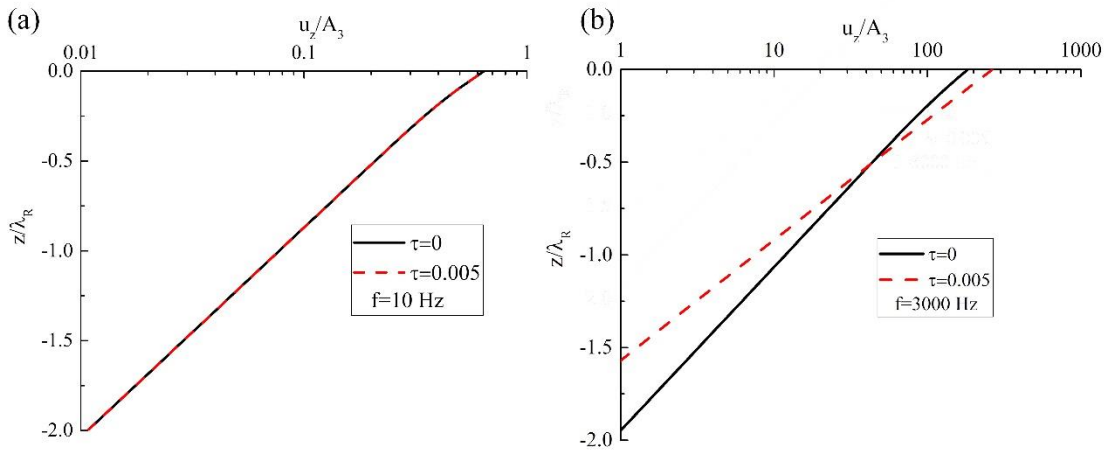

Fig. 5. Comparison of the vertical displacement at different frequencies for nonlocal parameters $\tau = 0\,\mathrm{m}$ and $\tau = 0.005\,\mathrm{m}$.